# Description of brain internal structures by means of spatial relations for MR image segmentation

Olivier Colliot, Oscar Camara, Rémi Dewynter and Isabelle Bloch

Ecole Nationale Supérieure des Télécommunications, Département TSI, CNRS UMR 5141
46, rue Barrault, 75634 Paris Cedex 13, France

## ABSTRACT

This paper presents a method for segmenting internal brain structures in MR images. It introduces prior information in an original way through descriptions of the spatial arrangement of structures by means of spatial relations, which are represented in the fuzzy set framework. The method is hierarchical as the segmentation of a given structure is based on the previously segmented ones. The processing of each structure is decomposed into two stages: an initialization stage which makes extensive use of prior knowledge and a refinement stage using a 3D deformable model. The deformable model is guided by an external force representing the combination of a classical data term derived from an edge map and a force corresponding to a given spatial relation. We propose different ways to compute a force from a fuzzy set representing a relation or a combination of relations. Results obtained for the lateral ventricles, the third ventricle, the caudate nuclei and the thalami are promising. The proposed combination of spatial relations and deformable models has proved to be very useful to segment parts of the structures were no visible edges are present, improving the segmentation accuracy.

**Keywords:** Spatial relations, brain imaging, segmentation, internal structures, deformable model

## 1. INTRODUCTION

The segmentation of brain internal structures such as the ventricles and the deep grey nuclei (caudate nucleus, putamen, globus pallidus, thalamus) has many medical applications such as morphometric studies, 3D visualization, surgical planning, anatomical support to functional studies ... However, their automatic segmentation in MR images remains a challenging task due to the image low-contrast and in some cases the lack of strong edges between some structures.

Several approaches dedicated to internal brain structures segmentation have been recently published. Most approaches rely either on a digital atlas which is registered with the image to be recognized[1–3] or/and on deformable templates[4–7] usually based on a statistical shape training. The main drawbacks of these approaches are the difficulty to deal with the anatomical variability among subjects and their computational cost.

Our approach uses descriptions of brain structures by means of spatial relations to constrain the segmentation procedure and a 3D deformable model to refine and to regularize the result. Spatial relations are less variable than the structures themselves which justifies to rely on them to constrain the search. Pitiot et al.[7] proposed an expert-knowledge guided segmentation system, combining distance relations with a deformable model for brain structures segmentation and showed improved segmentation results compared to the use of a deformable template. They combined both explicit (distance constraints) and implicit knowledge (shape constraints). In our case, we employ only explicit knowledge expressed through different kinds of spatial relations, including distances but also adjacency and directional relations. The relations are represented in a fuzzy set framework and are employed at three different stages of the process: to produce regions of interest (ROI) that will restrain the segmentation, to select regions that fulfill a description and to constrain the deformable model. The idea of using spatial relations in brain structures segmentation was first introduced by Géraud.[1,8] Nevertheless, in this system, ROI were built using a digital atlas, which may lead to some problems due to anatomical variability

Further author information: (Send correspondence to I.B.)
O.C.: Current address: McConnell Brain Imaging Center, Montreal Neurological Institute, McGill University, 3801 University, Montreal, Québec, H3A 2B4, Canada, colliot@bic.mni.mcgill.ca, Telephone: +1 514 398 8841
I.B.: E-mail: Isabelle.Bloch@enst.fr, Telephone: +33 1 45 81 75 85

among subjects. Moreover, this approach did not include a regularization phase which may compromise the segmentation of low-contrast structures. Another drawback of this strategy is the computational cost of the registration.

We propose a hierarchical procedure in which the segmentation of a given object makes use of information derived from previously obtained structures. After some preprocessing steps, the procedure is initialized by the segmentation of the lateral ventricles, which are the easiest brain internal structures to segment. Each structure is then segmented in two stages. The first step consists in a rough segmentation that will serve as initialization of the deformable model. First we compute a fuzzy region of interest (ROI) from spatial relationships guaranteeing that the object is included in it. After an automatic thresholding, we extract different regions of the expected radiometric class. Regions satisfying the description of the object to segment are then automatically selected and merged to produce an initial segmentation. In a second step, this initial result is refined and regularized using a deformable model.

The paper is organized as follows. In Section 2, we show how the arrangement of brain structures is described by means of spatial relations, how these relations are represented and used in the segmentation process. Then, in Section 3, we present the deformable model and the methods to compute an external force from the spatial relations. Finally some results are presented in Section 4.

## 2. SPATIAL RELATIONS

Spatial relations are used extensively in linguistic descriptions found in neuroanatomy textbooks. These descriptions correspond to structural relations between brain structures and are likely to be quite stable among subjects. They are naturally used by the neuroanatomist when studying an image. In this part, we first show how brain structures can be described using spatial relations and how this description can be formalized. We then introduce methods to represent spatial relations, based on the fuzzy set framework. Finally, we explain how those relations are used in the segmentation procedure.

### 2.1. Description of brain structures using spatial relations

In collaboration with a neuroanatomist (D. Hasboun, CHU La Pitié-Salpêtrière), we proposed a description of brain structures using spatial relations. It consists of a hierarchy of objects sharing relationships. Different levels of the hierarchy are linked by inclusion relations (e.g. the putamen is part of the basis nuclei which are part of the telencephalon), while objects of the same level are linked by spatial relationships. We use an anatomical hierarchy derived from the one proposed in Neuronames *.[9] The relationships are a computational formalization of linguistic descriptions given by the neuroanatomist. They include four types of relations: direction, adjacency, distances and symmetry. The 6 directional relations correspond to the 3 dimensions of the space: "above, below, in front of, behind, lateral, medial". The relations "lateral" and "medial", which are commonly used in anatomical descriptions, replace relations "left" and "right". This vocabulary is useful because the brain is approximately symmetrical with respect to the mid-sagittal plane, and by using these expressions, both hemispheres can be described in the same way. "Lateral" means "orthogonally and away from the mid-sagittal plane" while "medial" means "orthogonally and towards the mid-sagittal plane". Adjacency relations describe structures that are touching each other. Symmetry relations link homologous structures in both hemispheres. Finally, even though distance relations such as "close to", "far from" are not present in the original anatomical description, they have proved useful for the segmentation and have thus been added to the description. Here are some examples of anatomical descriptions using spatial relations:

- direction: the thalamus is lateral to the third ventricle and below the lateral ventricle;
- distance: the lateral ventricles are far from the brain surface;
- adjacency: the thalamus is adjacent to the third ventricle;
- symmetry: homologous structures of both hemispheres (e.g. left and right thalami) are approximately symmetrical with respect to the mid-sagittal plane.

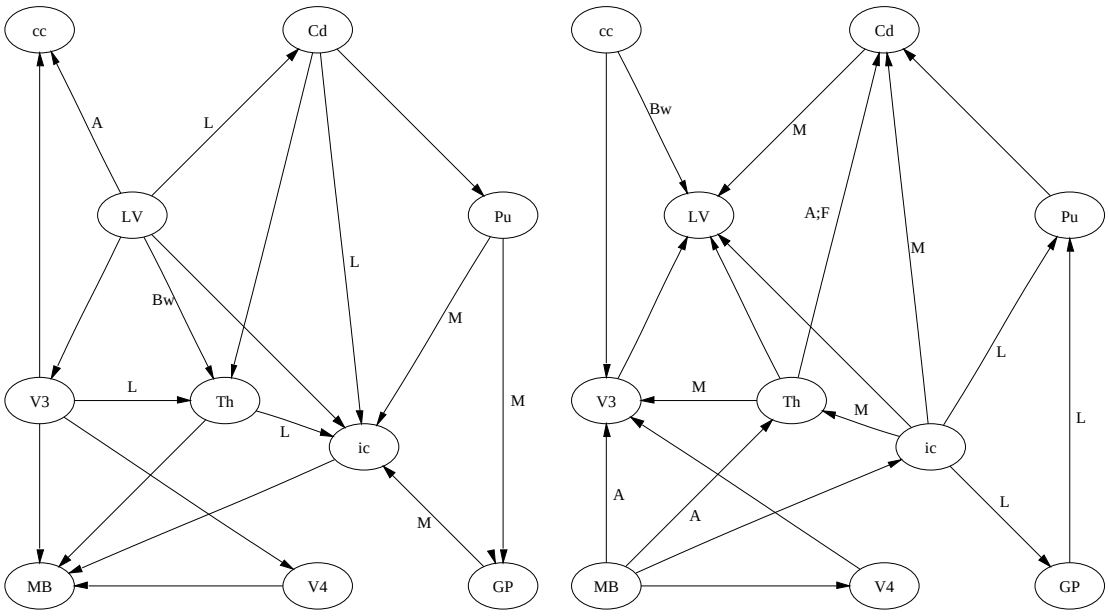


**Figure 1.** A fraction of the third level of the *synthetic hierarchical graph* describing brain structures. The following abbreviations are used for brain structures: cc - corpus callosum, LV - lateral ventricle, V3 - third ventricle, V4 - fourth ventricle, MB - mesencephalon, Cd - caudate nucleus, Pu - putamen, GP - globus pallidus, Th - thalamus, ic - internal capsule. Spatial relations are denoted as follows: I - medial, E - lateral, H - above, B - below, Av - in front of, Ar - behind. An edge between two structures indicates an adjacency relation. If the edge is attributed, there is an additional directional relation. The target object is at the end of the arrow: e.g. the relation $LV \xrightarrow{H} cc$ means that "the corpus callosum is above the lateral ventricle". To avoid conflicting edges and to enhance visualization, the graph is shown on two different figures, each one representing a fraction of the edges.

The anatomical description is formalized using a structure called a *synthetic hierarchical graph* (SHG). It is an attributed hierarchical graph, i.e. a set of graphs called *levels* such that the nodes of two consecutive levels are linked by inclusion relations. Each level has the structure of an attributed graph: the nodes correspond to brain structures and the edges to spatial relations between them. The SHG corresponding to brain structures contains 4 levels. A fraction of the third level, which contains the structures we want to segment (ventricles and grey nuclei), is shown as an example in Figure 1. Higher levels correspond to superstructures such as the telencephalon or the diencephalon. The lower level (level 4) corresponds to the subdivisions of structures such as, for example, the different horns of the lateral ventricle. The graph presented here has been used to represent brain anatomy but can be potentially used to describe any structured scene.

## 2.2. Representation of spatial relations

To handle imprecision, spatial relationships are represented in a fuzzy set framework and can refer to fuzzy objects as well as to crisp ones. This imprecision may come from either the processing of images or from the nature of the relations under consideration (e.g. directional relationships are intrinsically imprecise). Two kinds of fuzzy approaches can be used to represent spatial relations: one can define either a fuzzy set representing the degree of satisfaction of the relation with respect to a reference object in each point of the 3D space or a value representing the satisfaction of the relation between two given objects. The first approach presents several advantages: it allows the comparison of any target object with the reference one at a low computational cost, just by comparing the target and the fuzzy set, fusion operators can be used to combine spatial relations, the fuzzy set can also be considered as a ROI in which the target object should be found. The second approach consists in a direct comparison between objects and it can only be applied to the selection of regions.

*http://rprcsgi.rprc.washington.edu/neuronames/

Directions and distances have been represented using the first approach as in Bloch et al.[1] Directional relationships are represented by computing a fuzzy dilation of the reference object by a structuring element representing the direction under consideration. For distances, fuzzy sets representing linguistic descriptions such as *A is near B* or *A is at about 10 mm from B* are constructed on the set of distances $\mathbb{R}^+$. By combining them with distance maps, fuzzy sets in the 3D space are built. Examples of such fuzzy sets can be found in Figure 3. Adjacency and symmetry relations are represented using the second approach. An adjacency degree is defined using the method proposed by Bloch et al.[10] In the case of non-overlapping binary objects, this degree is computed as a function of the distance between objects. The symmetry measure[11] is defined as a measure of comparison between a given object and its symmetrical image with respect to a given plane, which, in our case, is the brain symmetry plane. This plane, which is a good approximation of the mid-sagittal plane, is found by maximizing a symmetry measure.[12] However, in our current implementation, symmetry relations are not used in the segmentation because brain hemispheres are treated separately. Only the brain symmetry plane is used, in order to separate the hemispheres. Nevertheless, as these relations can be integrated in the approach straightforwardly, we choose to present them in the paper.


**Figure 2.** Rough segmentation of the caudate nucleus (axial slices): (a) region of interest (ROI) corresponding to a conjunctive fusion with t-norm "product" of spatial relations: "lateral to the lateral ventricle" and "near the lateral ventricle"; (b) automatic thresholding in the ROI; (c) morphological opening of the previous result; (d) separation of the caudate and a fraction of the putamen; (e) rough segmentation; (f) simplex mesh corresponding to this rough segmentation.

### 2.3. Spatial relations application

Spatial relations are used in three different ways during the segmentation process: to define regions of interest (ROI), to select objects corresponding to a given description and to control the evolution of the deformable model. Let us first recall that each structure is segmented in two steps: a rough segmentation and a final segmentation. The first two applications of spatial relations occur only in the first step and are presented here while the third one, employed in the final segmentation, will be presented with the deformable model.

The first application of spatial relations concerns the construction of regions of interest to restrict the search of the structure to be segmented. When several spatial relations appear in the description of a structure, these relations are combined by means of fusion operators between fuzzy sets.[13] This is done using either a *t-norm* such as "minimum" or "product" in case of a conjunctive fusion. For a disjunctive fusion, a *t-conorm* will be adopted. This fusion operation provides a new fuzzy set which is used as a ROI to restrict the search of a given structure.

The second application is related to the selection of regions which have been labelled in the ROI. These regions are either connected components extracted after automatic thresholding or obtained from a watershed segmentation on the distance map to the contour of the class (the h-minima algorithm is used to remove irrelevant minima[14]) in case where different touching objects cannot be disconnected. When the selection involves distances and directions, we compute the degree to which a region satisfies the relation represented by a fuzzy set, using

a measure of satisfiability.[15] When the selection involves adjacencies and symmetries, a measure is directly available.

In order to clarify these two applications, we present an example corresponding to the rough segmentation of the caudate nucleus. First, using the "product" t-norm, we compute a ROI which corresponds to the following conjunctive fusion: "lateral to the lateral ventricle" and "near the lateral ventricle" (Figure 2(a)). An automatic thresholding is then performed in the ROI (Figure 2(b)). The threshold value is found by using an estimation of the radiometric characteristics of the grey nuclei due to Poupon,[16] which estimates the radiometry of the grey and white matter by the method of Mangin et al.[17] These values are not critical as the segmentation will be refined with the deformable model. After morphological opening (Figure 2(c)), the largest connected component, which corresponds to the caudate nucleus and a part of the putamen, is selected. Afterwards, the possible holes are filled by means of a morphological closing. A watershed segmentation on the distance map to the contour allows to separate the caudate nucleus from the putamen (Figure 2(d)). We then select the regions corresponding to the description of the caudate nucleus: these are the regions adjacent to the lateral ventricle and satisfying the previously fused relation. We obtain an initial segmentation (Figures 2(e) and (f)).

## 3. REFINEMENT USING A 3D DEFORMABLE MODEL

For most structures, the result obtained from the previous stage cannot be considered as a final result (see for example Figures 2(e) and (f)). In particular, the lack of regularization term may lead to imperfect boundaries. These problems are overcome using a deformable model.

### 3.1. Simplex mesh deformable model

All the structures in which we are interested have the topology of a sphere (except the third ventricle). To achieve a correct segmentation, we need to maintain their topology through the deformation process. This is performed with a discrete model based on simplex meshes. Simplex meshes, introduced by Delingette,[18] are topologically dual to triangulations and have a constant vertex connectivity. The segmentation obtained at the first stage is transformed to a triangulation using an isosurface algorithm based on tetrahedra.[19] It is decimated and converted to a simplex mesh by the dual operation (Figure 2(f)). Finally, its topological quality is optimized to make faces regular.

#### 3.1.1. Evolution

The evolution of the deformable surface $\mathbf{X}$ is described by the following dynamic force equation:

$$\gamma \frac{\partial \mathbf{X}}{\partial t} = \mathbf{F}_{int}(\mathbf{X}) + \mathbf{F}_{ext}(\mathbf{X})$$

where $\mathbf{F}_{int}$ is the internal force that specifies the regularity of the surface and $\mathbf{F}_{ext}$ is the external force that drives the surface towards image edges. The chosen internal force is:

$$\mathbf{F}_{int} = \alpha \nabla^2 \mathbf{X} - \beta \nabla^2 (\nabla^2 \mathbf{X})$$

where $\alpha$ and $\beta$ respectively control the surface tension (prevent it from stretching) and rigidity (prevent it from bending) and $\nabla^2$ is the Laplacian operator. It is then discretized on the simplex mesh using the finite difference method.[20]

#### 3.1.2. External Force

In our case, the external force is not only derived from image edges but also constrains the deformable model to satisfy the description of the structure. It can be written as a linear combination:

$$\mathbf{F}_{ext} = \lambda \mathbf{v} + \mu \mathbf{F}_R$$

where $\mathbf{v}$ is a Gradient Vector Flow (GVF) field introduced by Xu et al.[21] and $\mathbf{F}_R$ is the force attached to the spatial relationships described in Section 3.2. A GVF field $\mathbf{v}$ is computed by diffusion of the gradient vector of a given edge map and is defined as the equilibrium solution of the following diffusion equation:

$$\begin{cases} \frac{\partial v}{\partial t} = g(\|\nabla f\|)\nabla^2 v - h(\|\nabla f\|)(v - \nabla f) \\ v(x, y, z, 0) = \nabla f(x, y, z) \end{cases} \tag{1}$$

where $f$ is an edge map. In Section 3.3, we show how to construct an edge map suited to internal brain structures. Such a definition gives the GVF a large capture range and allows the model to progress into boundary concavities. The functions $g$ and $h$ are weighting functions which can be chosen as follows:

$$\begin{cases} g(r) = e^{-\frac{r}{\kappa}^2} \\ h(r) = 1 - g(r) \end{cases} \tag{2}$$

### 3.2. Deriving external forces from spatial relations

While in the two cases presented in Section 2.3 spatial relations were only involved in the initialization process, they can also be used to constrain the final segmentation. Applications of spatial relations in imaging available in the literature[1, 22, 23] make use of the relations only in the recognition phase, the segmentation part being achieved by classical techniques. Even in applications concerning segmentation, like in Bloch et al.,[1] spatial relations are not used to find the contour of the objects but, in that case, to select a radiometric class. However, in our case, the main difficulty lies in the lack of visible edges. For this reason, we propose to introduce spatial relations in a deformable model, through the definition of an external force derived from the fuzzy set. To our knowledge, the only combination of spatial relations and deformable models can be found in Pitiot et al.[7] However, the authors only consider the case of distance relations. Our approach, deriving a force from a fuzzy set, applies to any spatial relation that can be represented in this fuzzy set framework, including directional and distance relations.

The idea of deriving a force from a fuzzy set has already been used by Xu et al.[20] to reconstruct the cortical surface using a deformable model. But, in that case, the sets represented radiometric classes (of gray and white matters) derived from a fuzzy segmentation instead of spatial relationships. The authors used a balloon force, the magnitude of which was computed from the fuzzy sets:

$$w_p(x, y, z) = \begin{cases} 0 \quad \texttt{if } |2\mu_{wm} + \mu_{gm} - 1| \leq \delta \\ 2\mu_{wm} + \mu_{gm} - 1 \quad \texttt{elsewhere} \end{cases} \tag{3}$$

where $\mu_{wm}$ is the membership function of the white matter, $\mu_{gm}$ of the gray matter, and $\delta$ is a threshold. The direction of evolution ("inflate" or "deflate" the surface) is naturally determined in the previous equation. Indeed, $w_p$ is positive when the surface lies in the white matter, equal to zero when it is in the gray matter and negative when it is in the cerebro-spinal fluid or the background. In our case, to build a force corresponding to a given spatial relation $R$ represented by a fuzzy set of membership function $\mu_R$, we could choose $w_p(x, y, z) = 1 - \mu_R$. However, unlike in the previous case, there is no way to determine whether the surface should be "inflated" or "deflated", $w_p$ being positive. Thus, a balloon force does not appear to fit our needs. In the following, we propose three different ways to compute a force from a fuzzy set $R$ of membership function $\mu_R$.

In order to attract the deformable model in a region where the spatial relation is satisfied, the force should possess the following properties: be equal to zero where the relation holds (i.e. in the kernel of $R$), be non-zero elsewhere, be directed towards the points where the relation is satisfied and have a norm proportional to $1 - \mu_R$. If we used directly $P_R = 1 - \mu_R$ as a potential, the corresponding force $\mathbf{F}_R = -\nabla P_R$ would be obviously zero outside the support of $R$. This can be easily solved by adding to the potential the distance from the support, then defining:

$$P_R^1(x, y, z) = 1 - \mu_R(x, y, z) + d_{supp(R)}(x, y, z) \tag{4}$$

where $d_{supp(R)}$ is the distance from the support of $R$. With the following normalization, we obtain a force fulfilling our previous properties:

$$\mathbf{F}_R^1 = -(1 - \mu_R)\frac{\nabla P_R^1(x, y, z)}{\|\nabla P_R^1(x, y, z)\|} \tag{5}$$

A second way to define such a force would be to use a distance force[24] replacing the edge map with our fuzzy set. One has then to replace the classical distance with a distance from a fuzzy set, e.g. the morphological distance obtained by fuzzy dilation of the reference object.[25] However, this distance has a very high computational cost. Instead of that, we propose to use the distance to the kernel of $R$ which is a binary object:

$$P_R^2(x,y,z) = g(d_{Ker(R)}(x,y,z)) \tag{6}$$

where $d_{Ker(R)}(x,y,z)$ is a distance map to the kernel of $R$ and $g$ is a non-decreasing function, e.g. $g(x) = -ke^{-x^2}$ or $g(x) = -1/x$. The force $\mathbf{F}_R^2$ is derived through Equation 5.

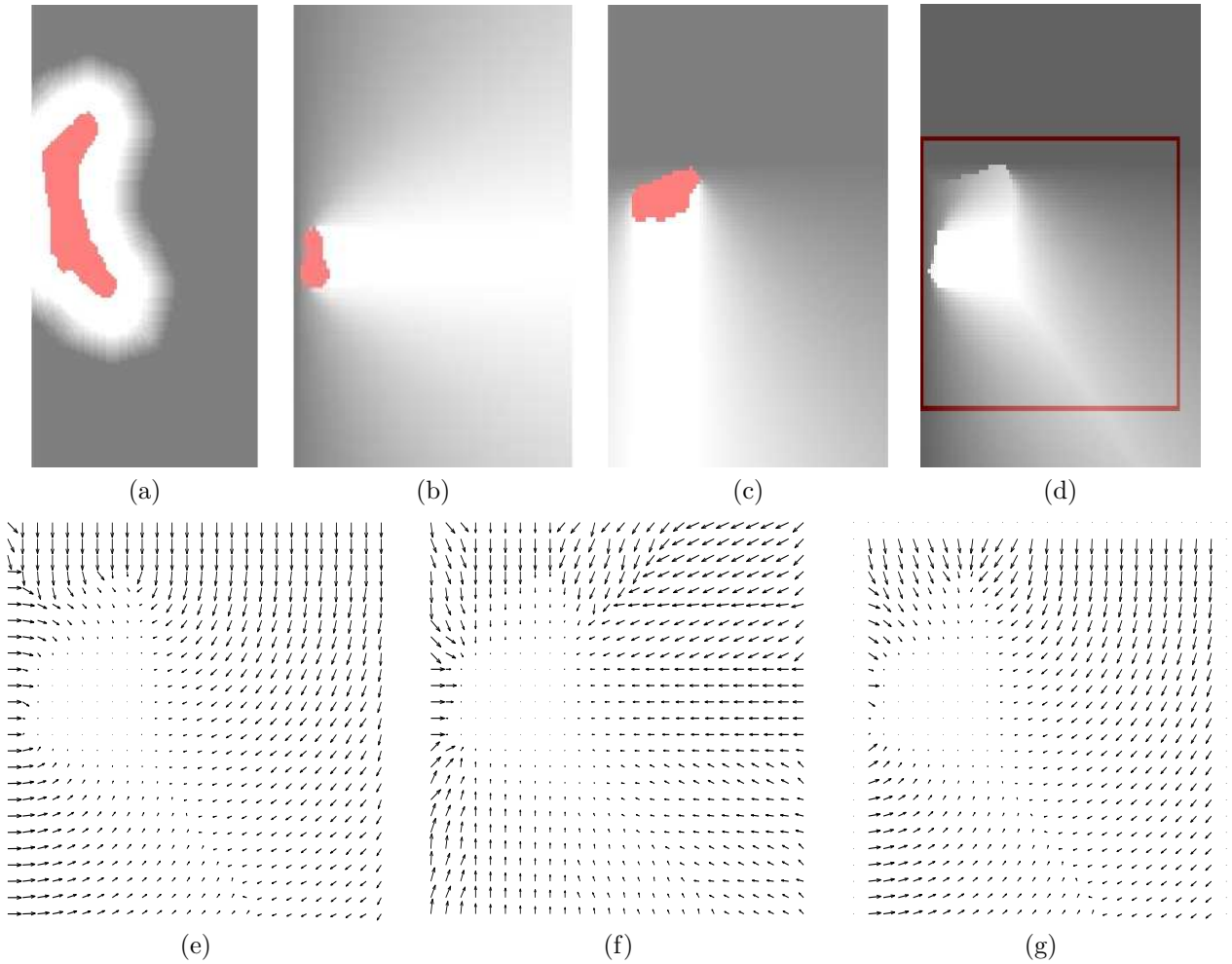


**Figure 3.** Slices of fuzzy sets representing spatial relations and the derived external force (only the part corresponding to the left hemisphere is shown): (a) distance: "close to the lateral ventricle", (b) direction: "lateral to the third ventricle", (c) direction: "below the lateral ventricle", (d) conjunctive fusion of the two previous directions, (e) external force corresponding to the fusioned relation, computed using the first method $\mathbf{F}_R^1$ (for visualization purposes a 1/3 undersampling has been performed and we only show the part of the previous image corresponding to the rectangle shown in (d)), (f) idem with the second method $\mathbf{F}_R^2$, (g) idem with the third method $\mathbf{F}_R^3$. Bright areas correspond to high values.

A third possibility is to use a gradient vector diffusion technique such as the Gradient Vector Flow (GVF). Again we have to replace the edge map with a fuzzy set, replacing $f$ with $\mu_R$ in Equation 1. However, the force would be non-zero in the kernel of $R$ which is a non desirable property. This can be solved using the following normalization:

$$\mathbf{F}_R^3 = (1 - \mu_R)\frac{\mathbf{u}}{\|\mathbf{u}\|} \tag{7}$$

where $\mathbf{u}$ is the GVF computed from the fuzzy set $R$.

Although they are similar, the 3 previous forces do not have exactly the same properties. In the particular case of a fuzzy set with local maxima outside its kernel, $\mathbf{F}_R^1$ and $\mathbf{F}_R^3$ would be directed towards these maxima whereas $\mathbf{F}_R^2$ would point towards the kernel of $R$. Figure 3 shows an example of each of these forces. One can see that $\mathbf{F}_R^1$ and $\mathbf{F}_R^3$ share a similar behavior. In particular, they are orthogonal to isolevels of $R$. This is not the case for $\mathbf{F}_R^2$ which is always directed towards the kernel. The computational cost of $\mathbf{F}_R^1$ and $\mathbf{F}_R^2$ is very low (5 seconds for a 128x128x124 image on a PC Pentium III 1Ghz). The computation time is higher for $\mathbf{F}_R^3$ (3 minutes), while being still acceptable. $\mathbf{F}_R^2$ should not be applied in case of fuzzy sets with maxima outside their kernel. It was not the case in our experiments and all forces have lead to extremely similar results. Finally, even though $\mathbf{F}_R^1$ and $\mathbf{F}_R^3$ are similar, $\mathbf{F}_R^3$ introduces a regularization which could be useful. It is also worth noting that all these results are valid in the case of a binary set instead of a fuzzy one. In that particular case, forces $\mathbf{F}_R^1$ and $\mathbf{F}_R^2$ would be equal as the kernel of a binary set is equal to its support.

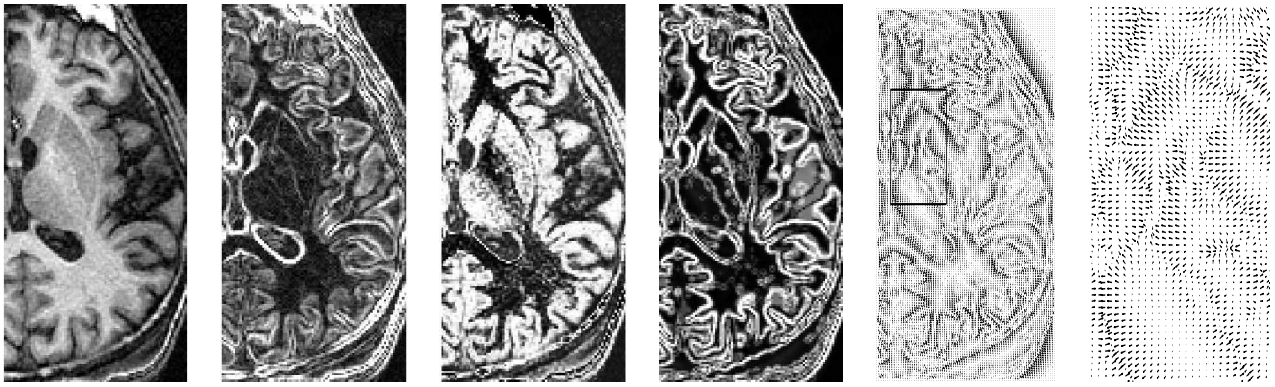


**Figure 4.** Edge map for the caudate nucleus (axial slices): (a) original image, (b) gradient computed on original image, (c) probability map, (d) edge map: gradient computed on probability map after anisotropic diffusion, (e) Gradient vector flow (GVF) computed on the previous edge map, (f) zoom on a portion of the GVF.

### 3.3. Edge map computation

Two main problems appear when computing an edge map associated to grey nuclei in MRI: the noise and the lack of contrast of the grey/white interface. Linear spatial filtering which is usually associated to Canny-Deriche edge detectors is inadequate in this case as it would mix contours of thin elongated objects such as those we are interested in. Anisotropic diffusion[26] is an efficient way to remove noise in homogeneous regions while preserving and even enhancing edges. However, due to the very tiny transition for some of the grey nuclei, this edge enhancement is insufficient.

We propose to use prior information on nuclei grey levels to enhance edges, computing the gradient on a probability map indicating for each voxel its membership to a given structure. This probability is computed as a distribution $P(x) = p(I(x))$ where $I$ is our image. Its gradient is related to the gradient of $I$ by $\nabla P(x) = p'(I(x))\nabla I(x)$. This means that edge enhancement will occur in the neighborhood of the extrema of $p'$. If we choose $p$ to be a Gaussian function $G_{m,\sigma}$ of mean $m$ and standard-deviation $\sigma$, edges will be enhanced in the neighborhood of $m \pm \sigma$. Parameters $m$ and $\sigma$ are estimated for each grey nucleus using the same method as in Section 2.3. To remove the noise, we finally apply an anisotropic diffusion on the probability map. Applying it on the map instead of the original image has the additional advantage to normalize the image, allowing to chose the same diffusion parameter for all images. Figure 4 presents an edge map computed for the caudate nucleus and the corresponding GVF.

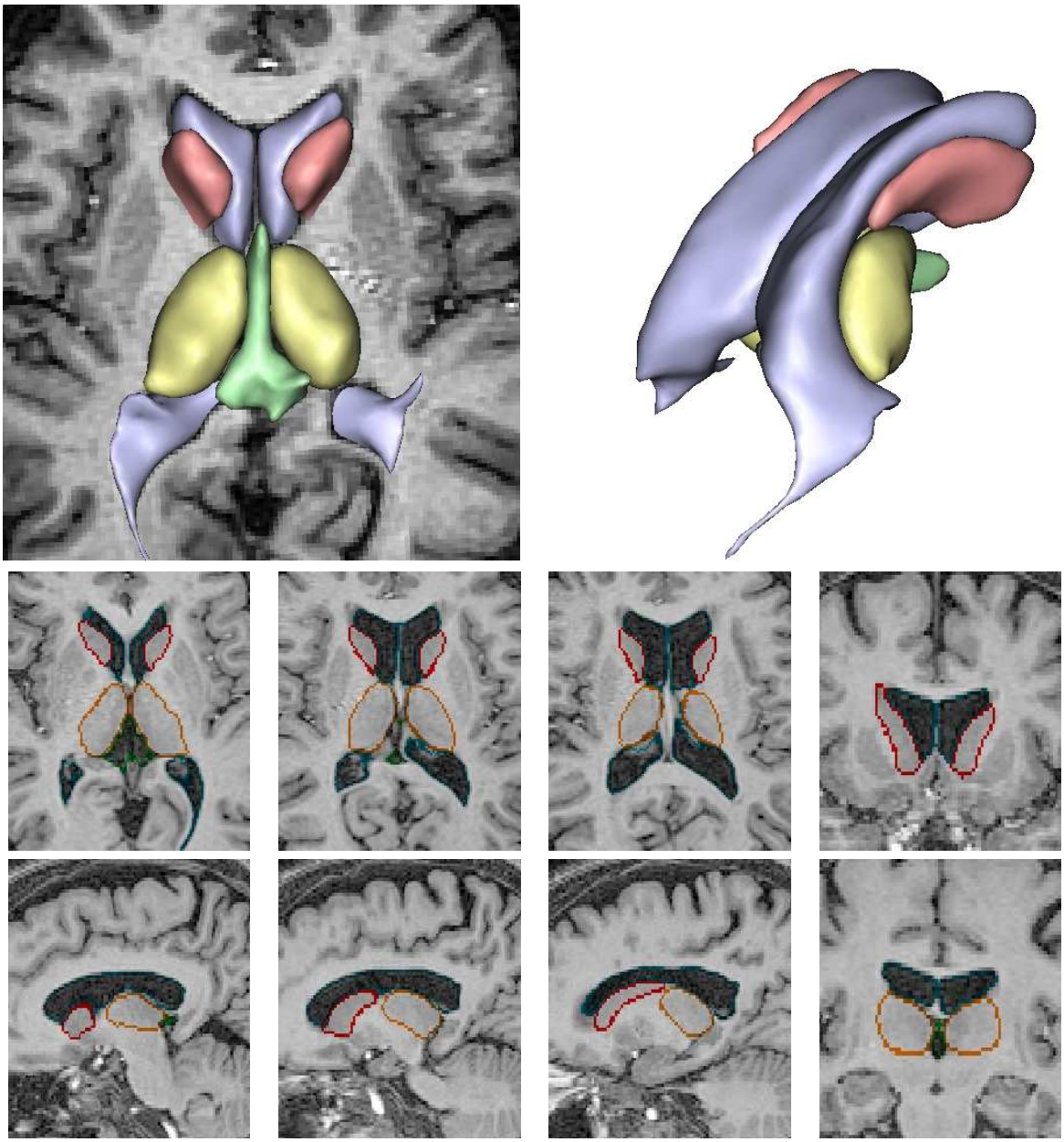

**Figure 5.** Results obtained for the lateral ventricles, the third ventricle, the caudate nuclei and the thalami. Top: 3D rendering superimposed on an axial slice. Bottom: structure contours superimposed on axial, sagittal and coronal slices. 3D images have been visualized using the Anatomist software (www.anatomist.info), developed at S.H.F.J, Orsay, France.

## 4. RESULTS AND CONCLUSION

All our experiments have been performed on T1-weighted MR images with size 256x256x124. Some preprocessing steps are needed. First, we correct the image for intensity non-uniformity.[27] Then, the brain is extracted using a robust method based on morphological operations.[17] This allows us to eliminate radiometric classes that are of no interest to our application (scalp, air, skull...). However, whereas we systematically use the non-uniformity correction before extracting the brain, we do not suggest to use it for the grey nuclei because their contrast seems to be altered by this correction. Finally, we compute the brain symmetry plane.[12]

We obtained good results for the ventricular system, the caudate nuclei and the thalami on a database

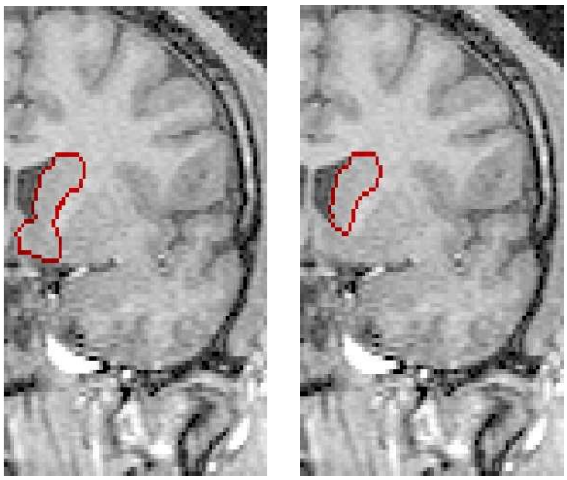

**Figure 6.** Influence of spatial relations on the evolution of the deformable model: segmentation of the caudate nucleus. The force corresponding to spatial relations prevents the model from evolving beyond the lower limit of the structure. Left: result obtained without spatial relation. Right: result obtained with the spatial relation.

containing 10 images (an example is shown in Figure 5). The ventricles are not very difficult to segment as they present a high contrast with surrounding structures. Only their separation is a bit more tricky, but this problem is solved by the watershed computed on the distance map to the contour. The ventricles, which are segmented first, are then used as a reference to segment the other structures. The lower part of the caudate nucleus is difficult to segment, due to the lack of gradients, and the trade-off between GVF and the spatial relations has shown to be useful in that case as can be seen in Figure 6. We are currently working on a more extensive validation of the method. The lower part of the thalamus is also difficult and in that case, the relation with respect to the third ventricle has helped to produce an acceptable rough segmentation. In order to compare our method to others, a quantitative validation is needed. At last, whereas the tuning of parameters has not been very difficult, a full study of their influence will be performed soon.

We proposed a method combining prior information derived from spatial relations and deformable models to segment brain internal structures in MRI. This information correspond to a description of brain anatomy and can be represented by a *synthetic hierarchical graph*. The combination of spatial relations and the deformable model is done through the introduction of a new external force. We proposed three methods to construct such a force. Good results have been obtained for the ventricular system, the caudate and the thalamus. We are now working on applying the method to other structures. They can include other grey nuclei such as the putamen and the globus pallidus but also white matter structures which are usually not segmented. Some limits of these structures are not visible on the MRI and in that case, spatial relations could be of great help. Mid-term perspectives of this work include the simultaneous segmentation of structures, which could lead to a greater robustness for structures such as the caudate nucleus, and also the combination of spatial relations and shape constraints in the deformable model.

## ACKNOWLEDGMENTS

We would like to thank Dr. Hasboun (CHU La Pitié-Salpêtrière) for providing the images and the descriptions of brain structures.

## REFERENCES

1. I. Bloch, T. Géraud, and H. Maître, "Representation and fusion of heterogeneous fuzzy information in the 3D space for model-based structural recognition - application to 3D brain imaging," *Artificial Intelligence* **148**, pp. 141–175, Aug. 2003.

2. B. Dawant, S. Hartmann, J.-P. Thirion, F. Maes, D. Vandermeulen, and P. Demaerel, "Automatic segmentation of internal structures of the head using a combination of similarity and free-form transformations: Part I, methodology and validation on normal subjects," *IEEE Transactions on Medical Imaging* **18**(10), 1999.
3. J.-H. Xue, S. Ruan, B. Moretti, M. Revenu, and D. Bloyet, "Knowledge-based segmentation and labelling of brain structures from MRI images," *Pattern Recognition Letters* **22**, pp. 395–405, 2001.
4. F. Poupon, J.-F. Mangin, D. Hasboun, C. Poupon, I. Magnin, and V. Frouin, "Multi-object deformable templates dedicated to the segmentation of brain deep structures," in *MICCAI 98*, *LNCS* **1496**, pp. 1134–1143, Springer Verlag, (MIT), Oct. 1998.
5. A. Kelemen, G. Szekely, and G. Gerig, "Elastic model-based segmentation of 3D neuroradiological data sets," *IEEE Transactions on Medical Imaging* **18**, Oct. 1999.
6. D. Shen, E. Herskovits, and C. Davatzikos, "An adaptative-focus statistical shape model for segmentation and shape modeling of 3D brain structures," *IEEE Transactions on Medical Imaging* **20**, Apr. 2001.
7. A. Pitiot, H. Delingette, N. Ayache, and P. Thompson, "Expert knowledge guided segmentation system for brain MRI," in *Medical Image Computing and Computer-Assisted Intervention MICCAI'03, volume 2879 of LNCS*, R. Ellis and T. Peters, eds., pp. 644–652, Springer-Verlag, (Montreal), Nov. 2003.
8. T. Géraud, *Segmentation des structures internes du cerveau en imagerie par résonance magnétique tridimensionnelle*. PhD thesis, Telecom Paris, 1998.
9. D. Bowden and R. Martin, "Neuronames brain hierarchy," *Neuroimage* **2**, pp. 63–83, 1995.
10. I. Bloch, H. Maître, and M. Anvari, "Fuzzy adjacency between image objects," *International Journal of Uncertainty, Fuzziness and Knowledge-Based Systems* **5**(6), pp. 615–653, 1997.
11. O. Colliot, I. Bloch, and A. Tuzikov, "Characterization of approximate plane symmetries for 3D fuzzy objects," in *Information Processing and Management of Uncertainty IPMU*, **3**, pp. 1749–1756, (Annecy, France), July 2002.
12. A. Tuzikov, O. Colliot, and I. Bloch, "Evaluation of the symmetry plane in 3D MR brain images," *Pattern Recognition Letters* **24**, pp. 2219–2233, Oct. 2003.
13. I. Bloch, "Information combination operators for data fusion: A comparative review with classification," *IEEE Transactions on Systems, Man, and Cybernetics* **26**(1), pp. 52–67, 1996.
14. P. Dokladal, I. Bloch, M. Couprie, D. Ruijters, R. Urtasun, and L. Garnero, "Topologically controlled segmentation of 3D Magnetic Resonance Images of the head by using morphological operators," *Pattern Recognition* **36**, pp. 2463–2478, Oct. 2003.
15. B. Bouchon-Meunier, M. Rifqi, and S. Bothorel, "Towards general measures of comparison of objects," *Fuzzy Sets and Systems* **84**(2), pp. 143–153, 1996.
16. F. Poupon, *Parcellisation systématique du cerveau en volumes d'intérêt. Le cas des structures profondes*. PhD thesis, INSA Lyon, Lyon, France, Dec. 1999.
17. J.-F. Mangin, O. Coulon, and V. Frouin, "Robust brain segmentation using histogram scale-space analysis and mathematical morphology," in *MICCAI 98*, *LNCS* **1496**, pp. 1230–1241, Springer Verlag, (MIT), Oct. 1998.
18. H. Delingette, "General object reconstruction based on simplex meshes," *International Journal of Computer Vision* **32**(2), pp. 111–146, 1999.
19. B. Piquet, C. T. Silva, and A. Kaufman, "Tetra-cubes: An algorithm to generate 3d isosurfaces based upon tetrahedra," in *SIBGRAPI 96*, **21**, pp. 205–210, 1996.
20. C. Xu, *Deformable Models with Application to Human Cerebral Cortex Reconstruction in Magnetic Resonance Images*. PhD thesis, Johns Hopkins University, 2000.
21. C. Xu and J. Prince, "Snakes, shapes and gradient vector flow," *IEEE Transactions on Image Processing* **7**, pp. 359–369, Mar. 1998.
22. F. Le Ber and L. Mangelick, "A Formal Representation of Landscape Spatial Patterns to Analyze Satellite Images," *AI Applications* **12**(1-3), pp. 51–59, 1998.
23. A. Perchant and I. Bloch, "A new definition for fuzzy attributed graph homomorphism with application to structural shape recognition in brain imaging," in *16th IEEE Intrumentation and Measurement Technology Conference*, **3**, pp. 1801–1806, 1999.

24. L. Cohen and I. Cohen, "Finite element methods for active contour models and balloons for 2D and 3D images," *IEEE Transactions on Pattern Analysis and Machine Intelligence* **15**(11), pp. 1131–1147, 1993.
25. I. Bloch, "On fuzzy distances and their use in image processing under imprecision," *Pattern Recognition* **32**(11), pp. 1873–1895, 1999.
26. G. Gerig, O. Kubler, R. Kikinis, and F. Jolesz, "Nonlinear anisotropic filtering of MRI data," *IEEE Transactions on Medical Imaging* **11**, pp. 221–232, June 1992.
27. J.-F. Mangin, "Entropy minimization for automatic correction of intensity non uniformity," in *MMBIA 00*, pp. 162–169, IEEE Press, (Hilton Head Island, South Carolina), 2000.